Elements of Solar Sail Navigation with Application to a Halley's Comet Rendezvous

Robert A. Jacobson* and Catherine L. Thornton†
Jet Propulsion Laboratory, Pasadena, Calif.

The problem of interplanetary navigation of a solar sail spacecraft is examined and found to be analogous to that of solar electric spacecraft. The dominant navigation error sources are shown to be accelerations that are unaccounted for in the description of the vehicle's motion, due to the inability to precisely model the solar radiation pressure. A strategy for navigation in the presence of these accelerations is devised, based on techniques previously developed for solar electric vehicles. An evaluation of the strategy is made for a Halley's comet rendezvous mission, and the results of that evaluation indicate that the strategy gives acceptable performance.

Introduction

A SOLAR sail spacecraft is one that uses a large reflecting surface to obtain a propulsive force from solar radiation pressure. The basic concepts underlying such a spacecraft are outlined in Refs. 1 and 2, along with a design for a "square sail" vehicle and a number of possible mission applications. In recent studies, both the square sail and an alternative design, the heliogyro,[3,4] were examined for possible development as an advanced propulsion vehicle. On the basis of design maturity and feasibility, reliability and simplicity, and manufacturability, the heliogyro appeared to be the most promising of the two designs. Consequently, the navigation concepts and analysis presented in this paper will implicitly assume the heliogyro design for the vehicle.

The heliogyro is a particular form of solar sail in which the reflecting surface is formed by a set of long, narrow, thin blades ($7500 \times 8 \times 2$m) rotating about a central axis, similar to a helicopter rotor. The centrifugal force generated by the rotation supports and stiffens the blades and keeps them in a flat plane. The blades are actively pitch-controlled, as with those of a helicopter, to provide attitude control, to provide thrust vector control by precessing the vehicle to change the orientation of the reflective plane relative to the sun, and to create small translational accelerations normal to and in the plane of the blades. These latter accelerations are quite useful from a navigation standpoint for the purpose of minor trajectory corrections.

An essential part of the solar sail feasibility studies is an investigation of the navigation problem associated with the vehicle. This paper discusses that navigation problem, describes a proposed navigation strategy, and evaluates it on a Halley's comet rendezvous mission, one of the most attractive among the many possible applications for a solar sail spacecraft.

The baseline design trajectory for a Halley's comet rendezvous[5] is composed of three distinct phases. The first phase is a transfer from Earth into a heliocentric circular orbit with a 0.25 A.U. radius. The second or cranking orbit phase is a rotation of the circular orbit about its line of nodes to obtain a final inclination of 146 deg. The third or rendezvous phase carries the spacecraft out of the cranking orbit and on to a postperihelion rendezvous with the comet at a heliocentric distance of about 0.97 A.U. During this phase, another 16 deg inclination is added to match the 162 deg inclination of Halley's orbit. Final encounter occurs at 100,000 km from the comet in the direction of the Sun with a final 200 m/s velocity toward the coment. Table 1 contains the basic mission parameters.

Received Sept. 23, 1977; revision received March 6, 1978.

Index categories: Spacecraft Navigation, Guidance, and Flight-Path Control; Electric and Advanced Space Propulsion.

*Member of Technical Staff, Systems Division. Member AIAA.
†Member of Technical Staff, Systems Division.

Solar Sail Navigation

Navigation Problem

Navigation encompasses two separate but closely related processes – orbit determination and guidance. The goal of the orbit determination process is to obtain knowledge of the spacecraft trajectory with sufficient accuracy, timeliness, and reliability that trajectory corrections and scientific instrument pointing can be successfully accomplished. The goal of the guidance process is to provide thrust vector control program corrections that will enable the spacecraft to follow a trajectory that is consistent with mission objectives and constraints. Orbit determination is basically the adjustment of the spacecraft state and the parameters in the dynamical and observational models until the difference between actual observations and those computed on the basis of the models are collectively minimized. Guidance is the adjustment of the parameters defining the thrust control program until the trajectory predicted by the dynamical model satisfies the trajectory requirements of the mission.

Successful navigation depends to a large extent on the accuracy of the mathematical models used; for the solar sail, one of the models of extreme importance is that of the radiation pressure which produces a significant nongravitational force on the vehicle. Errors in the solar

Table 1 Halley rendezvous trajectory characteristics

Launch date	Nov. 1, 1981
Launch energy (C_3)	12 km^2/s^2
Cranking orbit arrival	June 23, 1982
Cranking orbit departure	Aug. 18, 1983
Cranking orbit radius	0.25 A.U.
Time in Ø1 of trajectory	234 days (0.64 yr)
Time in Ø2 (cranking orbit)	421 days (1.15 yr)
Time in Ø3 (to encounter)	943 days (2.58 yr)
Begin final approach	E-100 days
Rendezvous date	March 19, 1986
Rendezvous distance from Sun	0.974 A.U.
Final inclination	162 deg
Total sail cruise time	1599 days (4.38 yr)
Trajectory bias	10^5 km toward Sun
Offset at rendezvous	200 m/s toward Halley

pressure model create unmodeled nongravitational accelerations which have three primary effects. First, they degrade orbit determination by placing a signature on the tracking data which cannot be adequately accounted for by the parameter adjustment process and may erroneously be attributed to significant trajectory dispersions. Second, they inhibit accurate prediction of future trajectory states and, consequently, have a direct effect on the computation of the thrust control law update. Finally, they cause the actual trajectory to deviate from the modeled trajectory, i.e., introduce trajectory dispersions.

The general nature of the solar radiation force acting on a spacecraft has been described,[6] and the force is commonly accounted for in the computation of ballistic interplanetary trajectories.[7] For ballistic spacecraft, the magnitude of the force is small, and modeling errors of a few percent lead to unmodeled accelerations of the less than 10^{-12} km/s^2, which can be accounted for in the orbit determination process. For the sail vehicle, on the other hand, solar pressure causes nominal accelerations of about 10^{-6} km/s^2 (at 1 A.U. from the Sun), and errors of only 1.0% yield unmodeled accelerations of 10^{-8} km/s^2, four orders of magnitude greater than those encountered on ballistic missions. Because of the complex nature of the solar pressure interaction with the sail vehicle, reduction of modeling errors to levels much below 1.0% may be extremely difficult. Sources of possible error are varied and numerous and can be grouped according to those resulting from an imperfect description of vehicle reflective properties and those resulting from inaccurate knowledge of the orientation of vehicle reflective surfaces relative to the Sun. Contributors to the former group may include: surface wrinkles and other local distortions; reflection coefficient dependencies on temperature and spectrum and incidence angle of incoming radiation; surface material creep and shrinkage due to temperature; surface distortion and flutter due to pressure loading; surface degradation due to cosmic rays, ultraviolet light, dust abrasion; and inexact integration of the local radiation pressure over the entire vehicle. Contributors to the latter group may include vehicle precession and nutation and blade pitch motor response.

Since it appears unlikely that solar sail unmodeled accelerations will be reduced to near-ballistic levels, they must be considered a major navigation error source. In fact, if they cannot be reduced at least three orders of magnitude, they will constitute the dominant navigation error source in a manner analogous to the thruster noise in solar electric propulsion navigation.[8-10] Consequently, the solar sail navigation problem is conceptually identical to that of solar electric, namely, navigation in the presence of high-level unmodeled accelerations; and the same techniques[8-10] proposed for solar electric can and must be applied to solar sail. These techniques include multistation radio data types, sequential estimation processes, and frequent trajectory corrections.

Navigation Strategy

Navigation strategy, i.e., the implementation of the orbit determination and guidance processes, involves the specific selection of data types and quantities, data processing procedure, control program update method and frequency, and control program update criterion. The fundamental element of the strategy for solar sail missions is the navigation cycle consisting of a tracking cycle, followed in turn by an orbit determination update and a thrust vector control program update and implementation. A tracking cycle is composed of four consecutive overlapping passes of dual frequency (*S*-band uplink and *S*- and *X*-band downlink) range and Doppler data with simultaneous Doppler and near-simultaneous range acquired during the overlapping view periods. The tracking cycle concept,[11] illustrated in Fig. 1, was developed for the Voyager mission to provide dual station data types. Since these data types are crucial to low thrust (solar electric/solar sail) navigation, the tracking cycle has

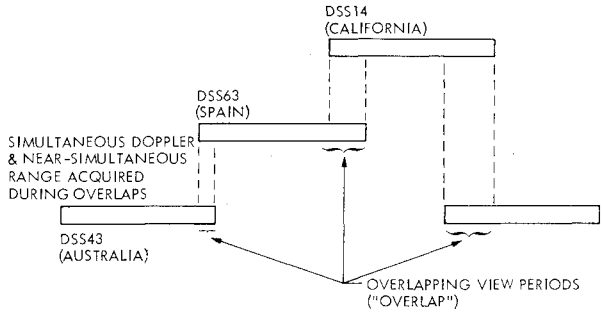

Fig. 1 Navigation tracking cycle (preferred stations shown).

been adopted as the basic means of obtaining radiometric data. It is preferred that each cycle begin and end with Australia in order to balance the northern and southern hemisphere coverage, since the long baseline between northern and southern stations enhances the effectiveness of simultaneous data. Because of its insensitivity to the high-level unmodeled accelerations, the simultaneous Doppler data may be considered the most important radiometric data type. During processing, it is explicitly differenced to further reduce its sensitivity to modeling errors and to remove common transmission media effects. Although differenced Doppler is normally two-way minus three-way data, during periods of near-solar conjunction differenced one-way *X*-band Doppler may be utilized instead. This data type avoids the problem of uplink phase scintillation which sometimes occurs in two-way/three-way data near-solar conjunction, yet it has the same inherent information content as the two-way minus three-way data. Explicit differencing removes the spacecraft oscillator noise. The use of dual frequencies, *S*- and *X*-band, provides a method for calibrating the effects of charged particles on the radio waves. This calibration is performed by utilizing the difference in the amounts of retardation due to charged particles in two signals transmitted simultaneously at different frequencies to assess the number of charged particles in the ray path.[12]

The orbit determination update includes not only the estimation of the current spacecraft position and velocity but also a refinement of the observational and dynamical models, particularly the sail force models. The update is performed using a sequential filtering procedure that also allows for the unmodeled accelerations by including them in the form of first-order Gauss-Markov stochastic processes. The mean values of these processes are included as estimated parameters to reduce the sensitivity of the orbit determination process to the model deficiencies.

The thrust vector control program update methods and criteria are dictated by the objectives of a particular mission. For example, on the proposed Halley comet rendezvous mission, the candidate methods and criteria are dependent on mission phase. Prior to cranking orbit insertion, the trajectory is to be retargeted at each update time for a satisfactory transfer into the cranking orbit. In the cranking orbit at each update, the thrust vector is selected to maximize the inclination rate while recircularizing the orbit to its normally planned radius. After leaving the cranking orbit, the trajectory is to be retargeted at each update for a minimum time rendezvous with the comet. A final retargeting is to be made at about 60 days from encounter and the resulting trajectory is then denoted as the nominal approach trajectory. Linear feedback gains for a minimum miss terminal guidance scheme[13] associated with that trajectory are to be computed and used to update the control program periodically throughout the approach phase. This form of approach guidance is planned because it is relatively simple operationally and avoids terminal controllability problems.

The frequency of navigation cycles is set by the frequency of the control program updates, which is determined by the

rate of trajectory dispersion growth, by the magnitude of the dispersions that can be corrected without encountering controllability limitations or unacceptable performance losses, by the need to prevent dispersions which violate mission constraints, and by operational considerations. For solar sail trajectories, dispersions increase at a rapid rate due to the unmodeled accelerations, and short-term correction capability is small because of the low level of thrust available from the sail. Consequently, if updates are infrequent, errors can become rather large and a significant time period will be required to remove them. On the other hand, frequent updates permit only small errors and maintain tight trajectory control, but place a heavy burden on the operation of the spacecraft. Clearly, a balanced update frequency must be set, and this frequency will be mission-dependent. It appears, in general, that rather large dispersions can be tolerated from a controllability standpoint during heliocentric cruise phases of a mission as long as retargeting is the adopted guidance method (Ref. 14 contains an analysis of this problem for solar electric vehicles). The update frequency for those phases will be chosen to maintain adequate performance for the mission. During approach, however, controllability becomes the driver for update frequency as the time remaining to remove errors becomes limited. The time between updates for that phase, therefore, must be set to restrict dispersion growth to a controllable level.

In addition to the data acquired within the tracking cycles, navigation in the approach phase of a mission also relies upon continuous conventional radio data between cycles and upon onboard optical observations of the target body. The optical observations provide a direct information link between the spacecraft and its target and have proved to be extremely useful,[10,15] especially for cases where the target body ephemeris uncertainty is large.[10] In fact, for cometary missions, the large comet ephemeris uncertainties would replace the unmodeled accelerations as the dominant error source if optical data were not included. For the Halley comet mission, the final retargeting at 60 days prior to encounter is to be based on an orbit determination solution that contains both optical and radio data in order to reduce the effect of Halley's ephemeris uncertainty and leave only small comet-relative trajectory dispersions to be corrected by the linear terminal guidance scheme.

Halley Comet Rendezvous Navigation Analysis

Proposed Navigation Strategy

The proposed baseline navigation strategy for the Halley comet mission is summarized in Table 2. The mission is divided into five phases: postlaunch calibration, heliocentric cruise from Earth to the cranking orbit, cranking orbit, heliocentric cruise from the cranking orbit to near encounter, and final approach. The basic data requirements and guidance techniques are outlined for each phase. The purpose of the postlaunch calibration phase is to monitor the initial performance of the sail and to refine the values of the parameters in the force model based on information gained from the tracking data. The other four phases have been discussed in general terms in the previous sections of this paper, and the table supplies the remaining implementation details (e.g., cycle frequencies and number and timing of optical navigation pictures).

Analysis Assumptions

For the evaluation of the strategy, navigation error sources include a priori spacecraft state errors for each phase, data errors, unmodeled accelerations, and, in the approach phase,

Table 2 Solar sail Halley comet mission navigation strategy

Period	Times, days	Data category	Guidance category	Description
Postlaunch calibration	L-0[a] to L + 14	Continuous *S*-band, tracking cycles	Open loop, fixed clock and cone angle	Continuous *S*-band Doppler and range, four evenly spaced tracking cycles; guide at preflight determined, fixed clock and cone angles to simplify calibration.
Heliocentric cruise-precrank	L + 14 to L + 345	Tracking cycles, differenced 1-way *X*-band	Target to cranking orbit entry	One tracking cycle every 2 weeks, differenced *X*-band at *S-E-P* angles <15 deg; guide by targeting to cranking orbit entry, target after each tracking cycle, select cranking orbit inclination for minimum total mission time.
Cranking orbit	L + 345 to L + 839	Tracking cycles, differenced 1-way *X*-band	Maintain optimum crank	Four evenly spaced tracking cycles per revolution with one cycle immediately preceeding each sail reorientation; differenced *X*-band at *S-E-P* angles <15 deg; guide by selecting clock and cone angles to maximize inclination growth while maintaining near circular 0.25 A.U. orbit, update angles after each tracking cycle.
Heliocentric cruise-postcrank	L + 839 to E-60[b]	Tracking cycles, differenced 1-way *X*-band	Target to rendezvous	One tracking cycle every 2 weeks, differenced *X*-band at *S-E-P* angles <15 deg; guide by retargeting to the minimum time rendezvous point, retarget after each tracking cycle.
Approach	E-60 to E-0	Continuous *S*-band, tracking cycles, onboard optical	Target to rendezvous, followed by minimum miss linear guidance	Continuous Doppler and range, one tracking cycle every 5 days, eight optical navigation pictures during the tracking cycle at E-60, 1 picture per day thereafter; guide by targeting to rendezvous after the cycle at E-60, then use linear, variable-time-of-arrival, minimum miss guidance with updates after each tracking cycle. For linear guidance use fixed control gains computed only once at the E-60 targeting.

[a] L = Launch. [b] E = Encounter.

Table 3 Standard deviations of a priori spacecraft state errors

Mission phase	Position, km	Velocity, m/s
Cruise (heliocentric)	30,000	100
Cranking orbit (heliocentric)	2,000	10
Approach (comet relative)	24,000	50

Table 4 Data error sources

Error source	Standard deviation
Radio data	
Station locations	
Spin axis	1.5 m
Longitude	3.0 m
Differenced range bias	5.87 m
Data noise	
Range rate	100 mm/s
Differenced range rate	1.0 mm/s
Range	1000 m
Differenced range	25 m
Optical data	
Camera biases	1 pixel (10 μrad)
Data noise	1 pixel (10 μrad)

Table 5 Cranking orbit data noise for differenced range rate

Cycle number	1.58 ISED model 1-σ noise, mHz	Differenced range rate 1-σ noise, mm/s
1	15	1.0
2	70	2.3
3	60	2.0
4	15	1.0
5	15	1.0
6	16	1.0
7	54	1.8
8	26	1.0
9	15	1.0

the comet ephemeris a priori uncertainty. The cruise analysis focuses on a 120-day portion of the trajectory which extended from E-1484 to E-1364 days, that period immediately preceding entrance into the cranking orbit. The cranking orbit strategy is examined on the first 105 days of the orbit (about 2-¼ revolutions), and the entire 60-day final approach phase is analyzed. The a priori state errors are given in Table 3. For the cranking orbit they correspond to cruise errors 1 day after a tracking cycle, i.e., those errors existing at the time of the implementation of a thrust vector control program update assuming a 1 day processing time. For approach, the a priori errors are the root sum square of the comet ephemeris uncertainties and heliocentric cruise errors existing just prior to a navigation cycle. The comet ephemeris uncertainties at the time of approach phase initiation are predicted to be 13,000 km in position and 2.3 m/s in velocity.[16]

Radio data errors are due to random noise, tracking station crust-fixed location errors, transmission media calibrations, Earth polar motion uncertainties, Earth spin rate variations, and range measurement biases. The transmission media effects, polar motion errors, spin rate errors, and range biases are all subject to calibration. However, since these calibrations are not exact, it is assumed for the purposes of analysis that the remaining errors, except for the range biases, can be combined with the station crust-fixed location errors to form equivalent station location errors. The range biases are modeled separately. Table 4 gives the magnitudes assumed for the various error sources. Noise levels used for the range and

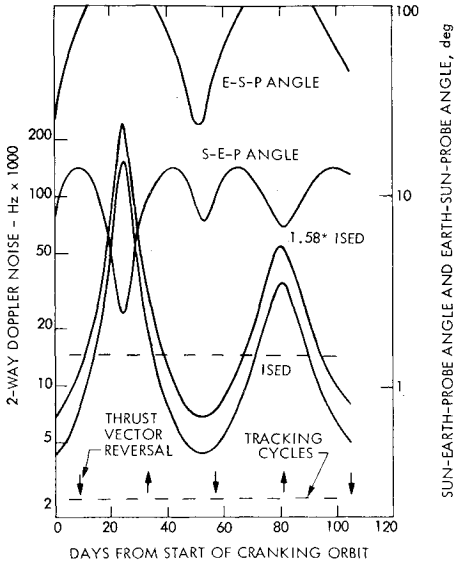

Fig. 2 Doppler noise, S-E-P angle, and E-S-P angle for the first 100 days of the cranking orbit.

range rate do not reflect the actual data accuracies, but rather were chosen to give the proper relative weighting between the conventional and differenced data types. Because several tracking cycles for the cranking orbit occur during periods of near-solar conjunction, the data noise on the differenced range rate for those cycles is varied to reflect the effects of the solar plasma. Based on the results of differenced Doppler demonstrations,[17] the differenced range rate noise levels are set at 50% of the two-way range rate noise levels predicted by the integrated solar electron density (ISED) model.[18] Figure 2 gives the range rate data noise according to the ISED model for the phase of the cranking orbit under investigation. Also shown are the Sun-Earth-probe angle, the Earth-Sun-probe angle, and the 1.58 ISED envelope which allows for uncertainties in the ISED model. It was the 1.58 ISED noise values which were actually used in determining the differenced range rate noise. Table 5 contains the noise levels used for each cycle in the cranking orbit analysis. The values correspond to either 50% of the maximum 1.58 ISED value within the tracking cycle or 1.0 mm/s, whichever is larger.

The major sources of error associated with optical data are TV distortions, image centerfinding errors, and random measurement noise. The distortions, which result from a number of electromagnetic and optical effects, corrupt the relative geometry of the images within a picture. The centerfinding errors, which are due to viewing finite size images, as well as image smearing by limit cycle motion, also hinder the determination of the relative geometry of the images. The distortions are subject to calibration, and for the purposes of this analysis, it is assumed that the post-calibration errors can be modeled as noise and angular biases of the order of the camera resolution. Because of the estimated small size of the comet nucleus (~5 km diam), centerfinding errors are assumed negligible. Table 4 contains the magnitudes used in the error models.

The unmodeled accelerations are accounted for by assuming independent random fluctuations in the characteristic acceleration‡ and the thrust vector clock and cone angles. Each of these fluctuations is represented by two first-order Gauss-Markov stochastic processes – one varying rapidly at the rotation rate of the vehicle, and a second varying more slowly at a rate related to the vehicle reorientation frequency and therefore different for each phase. The

‡The thrust acceleration of the spacecraft at 1 A.U. from the Sun with the sail oriented normal to the sun-line.

Table 6 Thrust error model parameters (standard deviation/correlation time)

Error source	Cruise	Cranking orbit	Approach
Long-term characteristic acceleration	1%/14 days	1%/1 day	1%/60 days
Short-term characteristic acceleration	1%/200 s	1%/200 s	1%/200 s
Long-term direction	1/4 deg/14 days	1/4 deg/1 day	1/4 deg/5 days
Short-term direction	1/4 deg/200 s	1/4 deg/200 s	1/4 deg/200 s

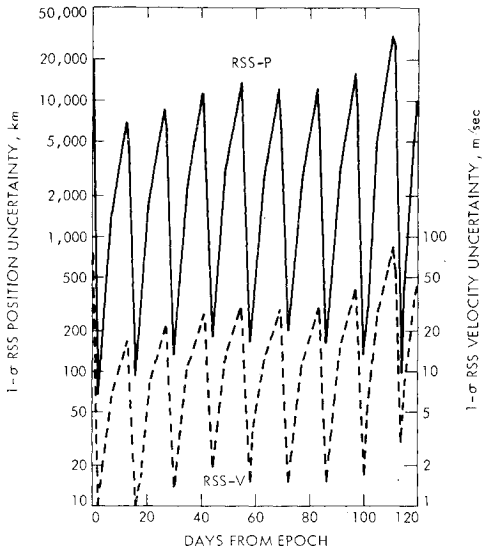

Fig. 3 Cruise orbit determination errors.

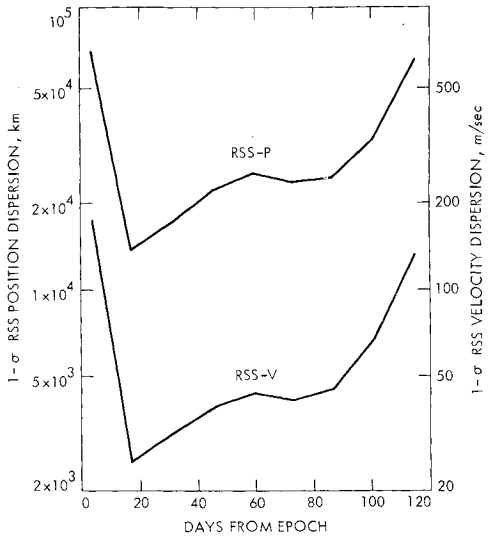

Fig. 4 Cruise dispersions at guidance update times.

magnitudes and correlation times of the processes are given in Table 6. It should be noted that the values of the thrust error model parameters and, in fact, even the structure of the error model itself, are very preliminary in nature and based primarily on intuition together with some sketchy error analysis. However, it is felt that the model is grossly representative of the type of thrust errors which can occur on a sail vehicle.

Analysis Results

For the cruise phase, Figs. 3 and 4 give the time histories of the orbit determination uncertainties and the dispersions existing at the guidance update times. The sawtooth pattern in the orbit determination results reflects the rapid orbit information degradation between cycles caused by the unmodeled accelerations. The dispersions of Fig. 4 are the orbit determination errors at the time of the previous guidance update mapped to the current guidance update and are primarily due to the cumulative effect of the unmodeled accelerations between updates. The rise in the dispersion errors near the end of the 120-day period is a consequence of the rise in the level of nominal thrust acceleration, and therefore a rise in the level of unmodeled accelerations as the spacecraft approaches the Sun.

The basic navigation accuracies for the cranking orbit are summarized in Table 7. The maximum and minimum orbit determination errors correspond to those at the start and end of each tracking cycle. As in the case of cruise, the dispersion errors are the trajectory errors at the time of each navigation cycle, due to the orbit determination errors remaining after the previous cycle plus the accumulated effect of unmodeled accelerations between cycles. Unlike the cruise results, the cranking orbit errors are essentially identical at each cycle time, because the magnitude of the sail force, and therefore of

Table 7 1-σ cranking orbit navigation errors

Error	Magnitude
O.D. errors	
Semimajor axis	
Min.	1450 km
Max.	55,800 km
Eccentricity	
Min.	0.000089
Max.	0.0017
Inclination	
Min.	0.0026 deg
Max.	0.037 deg
Dispersions	
Semimajor axis	66,300 km
Eccentricity	0.0020
Inclination	0.041 deg

Table 8 Cranking orbit correction accelerations

Acceleration component	Acceleration magnitude % of nominal (1-σ)	
	Stage 1	Stage 2
Radial	3.6	4.3
Transverse	0.6	0.2

Table 9 Final 1-σ delivery error breakdown

Errors	All error sources	Unmodeled accelerations	Other error sources
Position			
Downtrack	2322 km	2306 km	272 km
Crosstrack	2278 km	2275 km	117 km
Velocity			
Downtrack	1.57 m/s	1.54 m/s	0.31 m/s
Crosstrack	4.29 m/s	4.27 m/s	0.41 m/s
Time of arrival	1.19 h	1.18 h	0.15 h

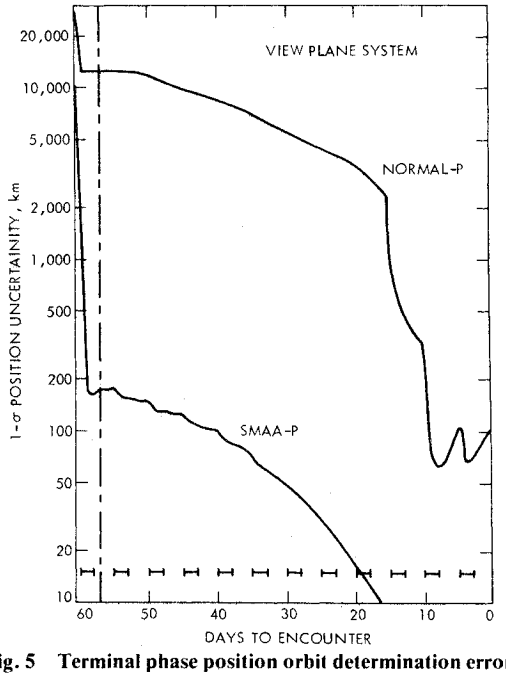

Fig. 5 Terminal phase position orbit determination errors.

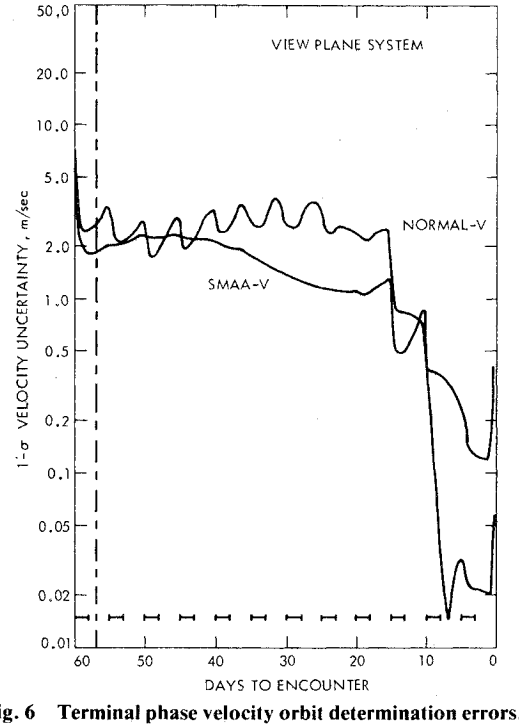

Fig. 6 Terminal phase velocity orbit determination errors.

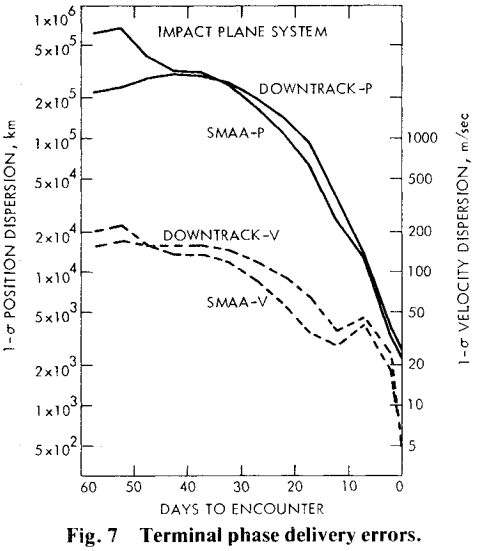

Fig. 7 Terminal phase delivery errors.

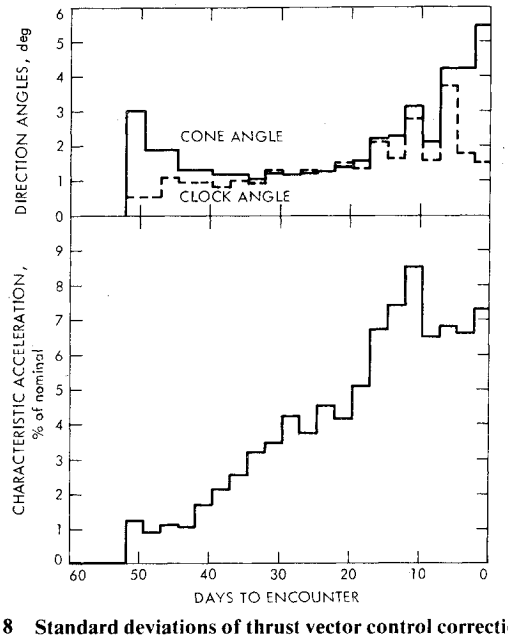

Fig. 8 Standard deviations of thrust vector control corrections.

the unmodeled accelerations, is nearly constant throughout the orbit. The level of the dispersion errors is within the 300,000 km tolerance required for adequate temperature control.

Table 8 gives the standard deviations of the trajectory correction accelerations generated by a candidate cranking orbit guidance law which nulls the semimajor axis and eccentricity dispersions while maximizing inclination rate. At each navigation cycle, the guidance law determines two successive radial and transverse (normal to the radius vector and in the instantaneous orbit) acceleration biases to be added to the nominal control program until the next cycle. Each bias is applied for 6 days, since the cycles are 12 days apart. The largest accelerations appear in the radial direction where they primarily control the semimajor axis dispersions. They are, however, less than 5% of the nominal acceleration level and are well within levels acceptable for navigational control.

Figures 5-7 summarize the approach navigation capabilities. The orbit determination results are displayed in the view plane coordinate system (the plane normal to the instantaneous spacecraft-comet line-of-sight) and include both the uncertainties at the final retargeting (E-57 days indicated by the vertical dashed line) and at subsequent times throughout the terminal phase. In the figures, "NORMAL" denotes the line-of-sight direction and "SMAA" the semimajor axis of the error ellipse in the view plane. The daily optical observations, together with the conventional radio data, cause the position errors, for the most part, to decrease monotonically. During the last 15 days, significant relative geometry changes lead to a dramatic improvement in errors normal to the plane. These errors are reduced to a level at which the effect of unmodeled accelerations becomes discernable, i.e., error growth between tracking cycles (indicated by the horizontal dashed line) can be seen. Throughout most of the approach, the velocity errors remain between 1.0 and 4.0 m/s, because the unmodeled accelerations inhibit the velocity determination from optical data which are position measurements. In fact, in the normal

direction, the weakest direction for optical data, the error growth between tracking cycles, is clearly evident.

The guidance results are displayed in the impact plane system (the plane normal to the comet-relative approach direction) and represent the delivery errors predicted at each update time, assuming no further trajectory correction. In the figure "DOWNTRACK" denotes the comet-relative approach direction and 'SMAA" the semimajor axis of the error ellipse in the impact plane. The control corrections computed at each update by the linear guidance law include variations in the thrust vector clock and cone angles and in the characteristic acceleration (implemented by blade feathering to alter the sail reflective area). The corrections are constant over 2.5-day intervals (i.e., two corrections are applied between updates) and their standard deviations are shown in Fig. 8. Because of the accumulated effects of unmodeled accelerations between the update times and encounter, the delivery errors are considerably larger than the orbit determination errors. The breakdown of the final 1-σ delivery errors into the contributions from the unmodeled accelerations and from all other error sources given in Table 9 clearly confirms this result.

Concluding Remarks

Unmodeled nongravitational accelerations dominate the problem of solar sail navigation in the same manner that they dominate the solar electric navigation problem. Consequently, previously developed techniques for solar electric missions are applicable to solar sail missions. A preliminary navigation strategy incorporating these techniques has been developed and analyzed for a Halley's comet rendezvous. The results of that analysis suggest that the solar sail can be navigated without significant difficulties. However, because this conclusion is based on the examination of a single mission, additional navigation assessments for other missions must be carried out before the navigability of the solar sail can be firmly established. Moreover, significant work remains to be done in the development of a realistic solar radiation force model, the calibration of that model, the characterization of the postcalibration modeling errors, and the effect of those errors on the navigation process.

Acknowledgment

This paper presents the results of one phase of research carried out at the Jet Propulsion Laboratory, California Institute of Technology, under Contract NAS7-100, sponsored by the National Aeronautics and Space Administration.

References

[1] Wright, J. L., "Solar Sailing: Evaluation of Concept and Potential," Batelle Memorial Institute Rept. No. BMI-NLVP-TM-74-3, Batelle Memorial Institute, Columbus Laboratories, Nov. 1974.

[2] Wright, J. L. and Warmke, J., "Solar Sail Mission Applications," AIAA Paper 76-808, San Diego, Calif., Aug. 1976.

[3] MacNeal, R. N., Hedgepath, J. M., and Schuerch, H. U., "Heliogyro Solar Sailer Summary Report," NASA-CR-1329, June 1969.

[4] MacNeal, R. H., "Structural Dynamics of the Heliogyro," NASA-CR-1745A, May 1971.

[5] Sauer, C. G., "A Comparison of Solar Sail and Ion Drive Trajectories for a Halley's Comet Rendezvous Mission," AAS Paper 77-4, Jackson Hole, Wy., Sept. 7-9, 1977.

[6] Georgevic, R. M., "Mathematical Model of the Solar Radiation Force and Torques Acting on the Components of a Spacecraft," JPL TM 33-494, Jet Propulsion Laboratory, Pasadena, Calif., Oct. 1971.

[7] Spier, G. W., "Design and Implementation of Models for the Double Precision Trajectory Program (DPTRAJ)," JPL TM 33-451, Jet Propulsion Laboratory, Pasadena, Calif., April 1971.

[8] McDanell, J. P., "Orbit Determination for Low-Thrust Spacecraft: Concept and Analysis," JPL TM-33-609, Jet Propulsion Laboratory, Pasadena, Calif., April 1973.

[9] Jacobson, R. A., McDanell, J. P., and Rinker, G. C., "Terminal Navigation Analysis for the 1980 Comet Encke Slow Flyby Mission," *Journal of Spacecraft and Rockets*, Vol. 11, Aug. 1974, pp. 590-596.

[10] Jacobson, R. A., McDanell, J. P., and Rinker, G. C., "Use of Ballistic Arcs in Low Thrust Navigation," *Journal of Spacecraft and Rockets*, Vol. 12, March 1975, pp. 138-145.

[11] Hildebrand, C. E., Ondrasik, V. J., and Ransford, G. A., "Earth-Based Navigation Capabilities for Outer Planet Missions," AIAA Paper 72-925, Palo Alto, Calif., Sept. 1972.

[12] Von Roos, O. H. and Mulhall, B. D., "An Evaluation of Charged Particle Calibration by a Two-Way Dual-Frequency Technique and Alternatives to This Technique," JPL TR 32-1526, Vol., XI, Jet Propulsion Laboratory, Pasadena, Calif., Oct. 1972, pp. 42-52.

[13] Jacobson, R. A., "A Constrained Discrete Optimal Guidance Strategy for Low-Thrust Spaceflight," AAS Paper, AAS/AIAA Astrodynamics Conference, Vail, Colo., July 1973.

[14] Fimple, W. R. and Van Dine, C. P., "Low-Thrust Guidance Study," Rept. E-910350-11, United Aircraft Research Laboratories, East Hartford, Conn.; Final Rept. for NASA Contract NAS8-20119, July 1966.

[15] Rourke, K. H., et al., "The Determination of the Interplanetary Orbits of Viking 1 and 2," AIAA Paper 77-71, Los Angeles, Calif., Jan. 1977.

[16] Yeomans, D. K., JPL Tracking Systems and Applications Section (private communication).

[17] Chao, C. C., JPL Navigation Systems Section (private communication).

[18] Berman, A. L. and Wackley, J. A., "Doppler Noise Considered as a Function of Signal Path Integration of Electron Density," *The Deep Space Network Progress Report 42-33*, Jet Propulsion Laboratory, Pasadena, Calif., June 1976.